J. Appl. Comput. Mech., 7(1) (2021) 93-101
DOI: 10.22055/JACM.2020.35250.2609

ISSN: 2383-4536
jacm.scu.ac.ir

Shahid Chamran University of Ahvaz

Journal of Applied and Computational Mechanics

Research Paper

Performance of Two Types of High Speed, High Efficiency Axisymmetric Intakes

Vladislav Galkin[1], Vasily Fomin[2], Sannu Mölder[3], Dmitry Vnuchkov[4], Valery Zvegintsev[5]

[1] School of Earth Sciences & Engineering, Tomsk Polytechnic University, 634050, Tomsk, Russia, Email: vlg@tpu.ru

[2] Khristianovich Institute of Theoretical and Applied Mechanics of the Siberian Branch of the Russian Academy of Sciences, 630090, Novosibirsk, Russia, Email: fomin@itam.nsc.ru

[3] Ryerson University, ON M5B 2K3, Toronto, Canada, Email: smolder@sympatico.ca

[4] Khristianovich Institute of Theoretical and Applied Mechanics of the Siberian Branch of the Russian Academy of Sciences, 630090, Novosibirsk, Russia, Email: vnuchkov@itam.nsc.ru

[5] Khristianovich Institute of Theoretical and Applied Mechanics of the Siberian Branch of the Russian Academy of Sciences, 630090, Novosibirsk, Russia, Email: zvegin@itam.nsc.ru

Received October 01 2020; Revised November 02 2020; Accepted for publication November 02 2020.
Corresponding author: Vladislav Galkin (vlg@tpu.ru)

Abstract. Performance of two axisymmetric air intakes are compared at conditions suitable for Mach number range from 2 to 8. First is the Busemann intake and second is the reversed isentropic nozzle. The isentropic nozzle is built by the method of characteristics. The contour of this nozzle is taken as a compression surface for the incoming flow. Performances of these two intakes are compared by comparison of both viscous and inviscid CFD calculations at Mach 6. Viscous flow calculations show that the total pressure recovery in compression section is 0.8316 in the Busemann intake and 0.869 in the reversed isentropic nozzle intake.

Keywords: Supersonic, Air intake, Near-isentropic compression, Total pressure recovery.

1. Introduction

The air intake of airbreathing engines is designed to capture atmospheric air, to reduce its speed by compression, and contraction and, with minimal loss of total pressure, supply it to the combustion chamber. The shape of the intake may be internal, external or a combination of the two. Intake shape determines the flow and shock structure and is therefore influential in determining the intake performance [1].

The design of air intakes is often based on selecting portions of simple (somehow symmetric), predictable and easily calculable flows. These flows have some degree of symmetry (planar, axial), reducing the number of independent spatial variables from three, by each symmetry degree. Examples of such commonly used simple flows are the flow behind a flat oblique shock, the Prandtl-Meyer flow, the conical flow and flow on an axisymmetric surface. Such flows have simple and easily predictable aerodynamic characteristics. Streamtubes that start from pre-assigned freestream capture shapes can be used to design wavecatcher intake surfaces that contain the simple flows [1, 2] and such, apparently three-dimensional streamtubes, can have swept leading edges that promote intake flow starting [3, 4]. Some of these simple flows, e.g. the Busemann, have unique characteristics that make them suitable for application to the design of supersonic and hypersonic intakes [5].

The first such air intake, with a section of isentropic compression, was proposed by A. Busemann [6]. Various aspects of the flow in the Busemann air intakes, including the start and un-start of the flow, the transformation of geometric shapes, the operation of the Busemann air intakes under off-design conditions (taking into account viscosity, angles of attack, truncation, changes in the Mach number, etc.) are considered in a large number of publications [2–5]. Subtle gas-dynamic phenomena occurring in conical flows in general and in the Busemann air intakes in particular, are considered in more detail in [5, 7, 8].

In the work [9], it was proposed to investigate air intakes with near-isentropic compression. Among them air intakes were considered where a leading edge angle was different from zero [10]. This made it possible to significantly reduce the length of the air intake and thereafter reduce the boundary layer losses. In this case, the flow began with a conical shock wave, which complicated the calculation of the flow field. The positive properties of such air intakes for hypersonic flight speeds were shown and examples of their construction were given. The air intakes were tested in aerodynamic wind tunnels [10, 11]. In work [12–14], the study of isentropic compression continues to improve the characteristics of air intakes for supersonic and hypersonic flight speeds.

A new approach to the design of isentropic flows and supersonic air intakes with isentropic compression was proposed in [15–18]. The essence of this approach is to design an isentropic flow in an axisymmetric supersonic expanding nozzle and then

Published online: November 16 2020

reverse the flow to create a compressive and contractive streamtube, suitable for use as an air intake. Such an air intake is called here *Reversed Isentropic Nozzle* - RIN intake. The task of forming a supersonic air intake, based on an annular nozzle with a profiled central body was considered in [15]. In [16], along with the central body, the outer wall was also profiled, and a comparison with the same initial parameters with a classical nozzle without a central body showed that the classical nozzle is longer. In [17, 18], inversed annular nozzle contours were used to develop air intake contours which provide the desired exit flow parameters.

This paper presents the methods of calculating the contours of the Busemann and RIN surface shapes, it compares their performance, as intakes, by both inviscid and viscous CFD calculations.

2. Equations Governing Axisymmetric Supersonic flow

The axisymmetric supersonic air flow in the Busemann and RIN intakes are based on the irrotational, steady, axisymmetric flow of a perfect ideal (inviscid, non-conducting) gas, which is described by the following system of equations:

$$\begin{aligned}
&\frac{\partial(y\rho u)}{\partial x}+\frac{\partial(y\rho v)}{\partial y}=0,\\
&\frac{\partial[y(\rho u^2+p)]}{\partial x}+\frac{\partial(y\rho uv)}{\partial y}=0,\\
&\frac{\partial(y\rho uv)}{\partial x}+\frac{\partial[y(\rho v^2+p)]}{\partial y}=p,\\
&\frac{\partial(y\rho uH)}{\partial x}+\frac{\partial(y\rho vH)}{\partial y}=0.
\end{aligned} \tag{1}$$

The total enthalpy has the form,

$$H=\frac{\gamma}{\gamma-1}\frac{p}{\rho}+\frac{w^2}{2}. \tag{2}$$

Where x, y are longitudinal and transverse axis of the cylindrical coordinate system; ρ is gas density; u, v are components of the gas velocity in the projection on the axis x and y; p is gas pressure; γ is specific heat ratio. The following notation is used below: $\delta=\arctan(v/u)$ is angle between the velocity vector and the x-axis; $w^2=u^2+v^2$; w is gas velocity; $a=\sqrt{\gamma p/\rho}$ is sound velocity; $M=w/a$ is Mach number; $\mu=\arcsin(1/M)$ is Mach angle. The boundary condition on the wall (streamline) is defined by: $dy/dx=v/u$, here $y(x)$ is wall generatrix. The remaining boundary conditions are discussed below.

3. The Busemann Intake

A diagram of the Busemann intake flow features is shown in Fig. 1. The compression surface of the intake has a zero initial angle relative to the freestream velocity vector of the incident uniform flow. It contains an isentropic axisymmetric conical flow which decelerates and flows towards the axis, ending at a conical shock wave. The flow is then deflected through the shock to become a uniform and parallel flow at the exit of the intake.

Figure 1 shows only some of the $C^{\pm}$ characteristics. At the entrance to the Busemann intake there is a uniform rectilinear characteristic C^-. The C^- characteristics from the leading portion of the surface converge onto the focal point of the Busemann flow. For details, see [5]. The Busemann air intake is based on a conical axisymmetric flow that obeys the Taylor-Maccoll equation [19], the same equation is used to calculate the supersonic flow around of the circular cone [20]. The flow pattern in the Busemann air intake is shown in Fig. 2.

Busemann air intake shape is calculated as in [5, 6, 21, 22]. A spherical coordinate r is radius vector and θ is spherical angle are introduced. The flow is isentropic and conically symmetric with the flow parameters depending only on θ. Initial spherical angle θ_b corresponds to the angle between the conical shock and the x-axis. The final spherical angle, from Fig. 2, is $\theta_d=\pi-\arcsin(1/M_1)$.

The velocity components were introduced: V_θ is normal to the radius vector and V_r is tangent to radius vector. In addition, dimensionless velocities U and V were introduced in the following way:

$$U=\frac{V_r}{W_{max}}, V=\frac{V_\theta}{W_{max}}. \tag{3}$$

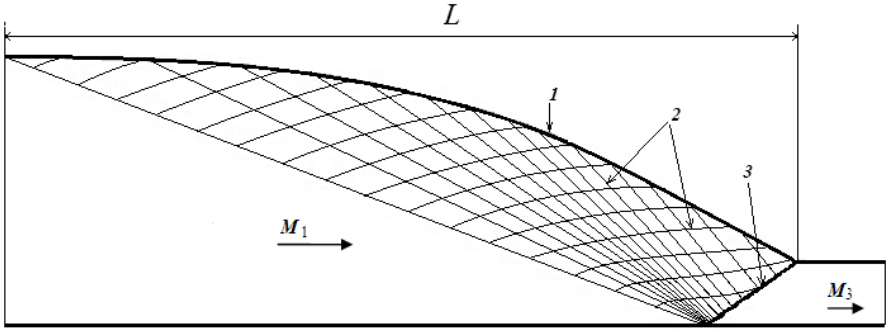

Fig. 1. Scheme of the Busemann intake [5], L is the length of the compression surface, 1 is compression surface, 2 are characteristics of $C^{\pm}$, 3 is conical shock wave, M_1 is Mach number of uniform flow in the entry cross section, M_3 is Mach number of uniform flow at the exit

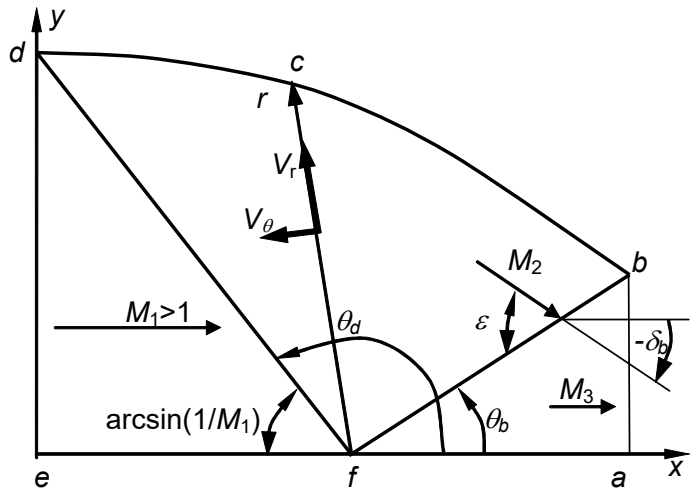

Fig. 2. Flow pattern in the Busemann air intake. *ed* is entry cross section with uniform flow and Mach number M_1; *dcb* is Busemann air intake contour; *f* is center of spherical coordinates *r* and θ on surface *xy*; *r* is radius vector; θ is spherical angle; *fb*, *fd* are respectively initial and final radius vectors; θ_b, θ_d are respectively, the initial and final spherical angles; *fd* is characteristic C^- to the left of which the flow is uniform; *fb* is conical shock wave (Busemann shock), to the right of which the flow is uniform; θ_b is angle between the shock wave and the x-axis; M_2 is Mach number at the front of the shock; M_3 is Mach number of uniform flow after shock; ε is Busemann shock angle; *ab* is uniform exit flow; δ_b is flow deflection through the Busemann shock

Here W_{max} is the maximum velocity that can be obtained from expression (2), given that *H*=const and *p*=0. Next, the relationship between the velocity components was used:

$$\frac{dU}{d\theta} = V. \tag{4}$$

As shown in [23], taking into account (3), (4), from a system of partial differential eqs. (1) for a conical flow, one obtains a dimensionless nonlinear ordinary second-order differential Taylor-Maccoll equation [19]:

$$\frac{\gamma-1}{2}\left(1-U^2-\left(\frac{dU}{d\theta}\right)^2\right)\left(2U+\frac{dU}{d\theta}\cot\theta+\frac{d^2U}{d\theta^2}\right)-\left(\frac{dU}{d\theta}\right)^2\left(U+\frac{d^2U}{d\theta^2}\right)=0.$$

For this equation there are the following boundary conditions. A uniform flow is specified at the entry, respectively, on the straight line *fd*, the Mach number M_1 and the zero slope of the streamlines are specified. At the exit, the Mach number M_3 and the zero slope of the streamlines are set, respectively, on the straight line *ab*. There will be two parameter values on the straight line *fb*. One set of parameters will be at the front of the shock, the second set of parameters corresponds to the position after the shock:

$$M_{fd} = M_1, \qquad M_{fb-} = M_2, \qquad M_{fb+} = M_{ab} = M_3, \qquad \delta_{fb+} = \delta_{ab} = \delta_{fd} = 0.$$

Relations on the conical shock wave are used that connect the parameters at the front and behind the front of the conical shock wave.

4. RIN Intake

We posit the fact that the isentropic flow of expansion in a diverging axial nozzle can be reversed to form the compressible flow in a converging air intake. The shape of the nozzle and intake are identical, the flows are the same (only reversed in direction) and both flows have no shock waves (see Fig. 3). The axial nozzle can be calculated by the method of characteristics, assuming steady flow of a perfect ideal (inviscid, non-heat-conducting) gas.

Figure 3 shows a nozzle with supersonic flow, from right to left, and characteristics depicted by the dashed lines emerging from the corner point of the nozzle in a centered Prandtl-Meyer-like rarefaction wave that reflects from the axis.

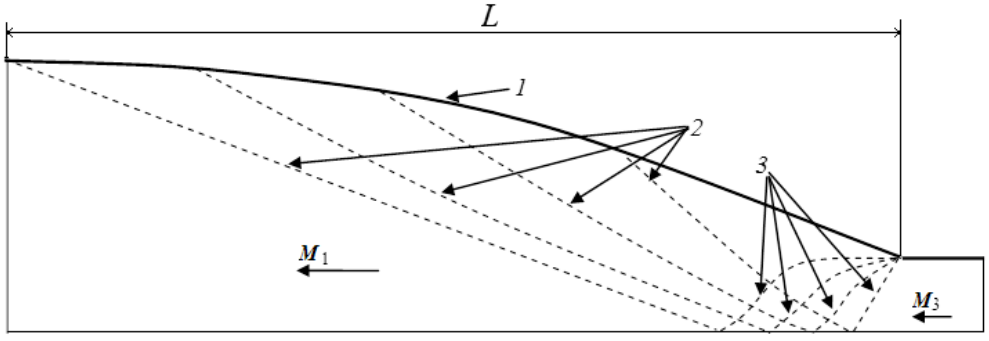

Fig. 3. Isentropic nozzle with a corner point. *L* is the length of the nozzle, *1* is nozzle surface, *2* are characteristics C^+, *3* are characteristics C^-, M_1 is Mach number of uniform flow in the exit cross section, M_3 is Mach number of uniform flow in the entry cross section

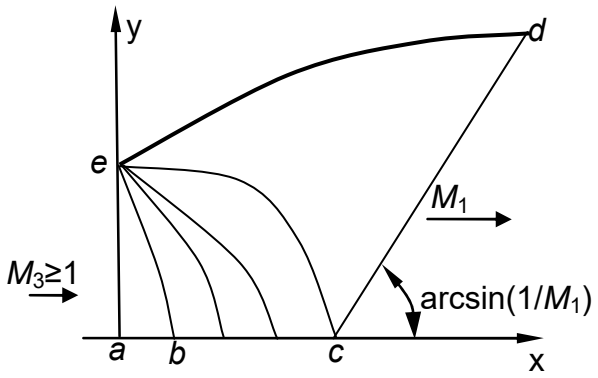

Fig. 4. Flow pattern in the axial nozzle with a uniform exit flow. *ae* is flow entry cross section with uniform flow and Mach number M_3; *ed* is nozzle contour with a corner point in a minimum section; *cd* is closing uniform characteristic C^+ with Mach number M_1; *be* is initial characteristic C^-; *bec* is centered rarefaction wave arising from the flow around a corner point *e* (only C^- family characteristics are shown); *ec* is last characteristic in rarefaction wave

The last characteristic in the rarefaction wave, after reflection from the axis, is uniform and straight. The contour of this nozzle is taken as a compression surface for the incoming flow, from left to right, of a new air intake as a reversed isentropic nozzle (RIN). The RIN intake, in the form of a reversed nozzle, is based on an axial supersonic nozzle with a parallel and uniform exit flow. When the flow is reversed in the nozzle, which now plays the role of an air intake, a shock waves and total pressure losses are possible in this compression region.

The profile of this nozzle is calculated by the method of characteristics. For supersonic flow, constant entropy and total enthalpy, in eqs. (1), the equations of the characteristics $C^{\pm}$ and the compatibility conditions are:

$$\frac{dy}{dx} = \tan(\delta \pm \mu), \qquad d\delta \pm \frac{\cos^2\mu}{(\gamma+1)/2 - \cos^2\mu} d\mu \pm \frac{\sin\mu\sin\delta}{y\cos(\delta \pm \mu)} dx = 0. \tag{5}$$

If dx=0, then the compatibility conditions are integrated, and the Prandtl-Meyer equation is obtained.

Based on the approach described in [24], and using relations (5), a supersonic nozzle of the smallest length [25] is computed, which makes it possible to transform a uniform flow with one Mach number M_3 into a uniform flow with another (larger) Mach number M_1. Figure 4 shows a nozzle contour with a uniform exit flow.

The main stages of the calculation are as follows. At the entrance to the nozzle *be* is initial characteristic C^- is established. From it, a centered rarefaction wave is calculated, which occurs during the flow turn around the corner point *e*. This calculation is completed, when calculating the last characteristic *ec* it yields the given Mach number M_1. From point *c* uniform characteristic C^+ is issued, and in the characteristic triangle *ecd* a characteristics network is calculated. A streamline, *ed* can now be drawn, in the characteristics network, from the corner point. It yields a nozzle with a corner point. A more detailed description of the method of characteristics is given in [15, 26, 27].

5. Numerical Simulation of the Flow in the Air Intakes

To analyze the behavior of the viscous supersonic flow in the air intakes, the viscous and inviscid flows were simulated without wall heat exchange. The 2D computational model was plotted in the software complex CAD SolidWorks. Then this model was imported to the standard computational mesh builder ANSYS Meshing. A structured grid was built with increasing refinement towards the wall of the air intake. The final grid had 30,000 cells.

The calculation region is bounded by the plane of symmetry. The right boundary is the end of model. On the left boundary the initial conditions are given. On the walls of the channel the no-slip conditions were set. The walls were assumed to be adiabatic. At the beginning of the calculation the entire area was filled with the conditions in the incoming flow. A stationary flow was used.

The calculations were performed by integrating of Reynolds averaged Navier-Stokes equations describing the flows of a viscous compressible gas using the software package ANSYS FLUENT. As a model of turbulence, the SST model was chosen. The SST model has the following features: it is a hybrid model - in the near-wall region, a k-ω turbulence model is used, while in the outer flow, the k-ε model is used. The calculation was carried out using a finite volume method based on the solution of the equation for density (Density-Based). Also parts of the calculations are performed using an inviscid model.

The viscous flow calculations are carried out with the parameters of the incoming flow corresponding to the standard atmosphere at the Earth's surface: the pressure P = 101325 Pa, the temperature T = 293 K, the Mach number M_1 = 6, the intake entrance diameter D = 0.2 m. Reynolds number based on entry diameter was equal Re_D=27.4×10^6.

5.1 Comparison of air intakes

The shape of the Busemann air intake was calculated as a solution of the Taylor-Maccoll equation, and the axisymmetric RIN intake by the method of characteristics in the Mach number ranges $2 \le M_1 \le 8$ and $1 \le M_3 \le 5$ for $\gamma = 1.4$. Maximal length of intakes is reached when Mach number at the intake exit is equal to $M_3 = 1$ (see Fig. 5). Comparison of computed profiles shows that, in almost the entire considered range of Mach numbers of the incoming flow, M_1, the length of the RIN intakes exceeded the length of the Busemann air intakes by about 0.5*D*.

The total pressure loss in the oblique shock of the Busemann air intake reaches a maximum when $M_3 = 1.0$, where the total pressure recovery coefficient is from 0.992 at $M_1 = 2.0$ to 0.658 at $M_1 = 8.0$. With an increase in M_3, the losses in the oblique shock decrease markedly, and at $M_3 = 3.0$ the recovery coefficient exceeds 0.922 in the entire range of considered values of M_1 (see Fig. 6). In the same range, there is theoretically no loss of total pressure in the RIN intake.

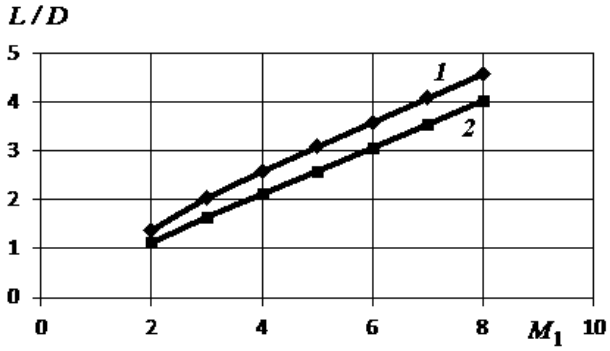

Fig. 5. Maximal length of the air intakes with M_3=1 at the intake exit. 1 is RIN intake; 2 is Busemann intake; M_1 is Mach number of the incoming flow

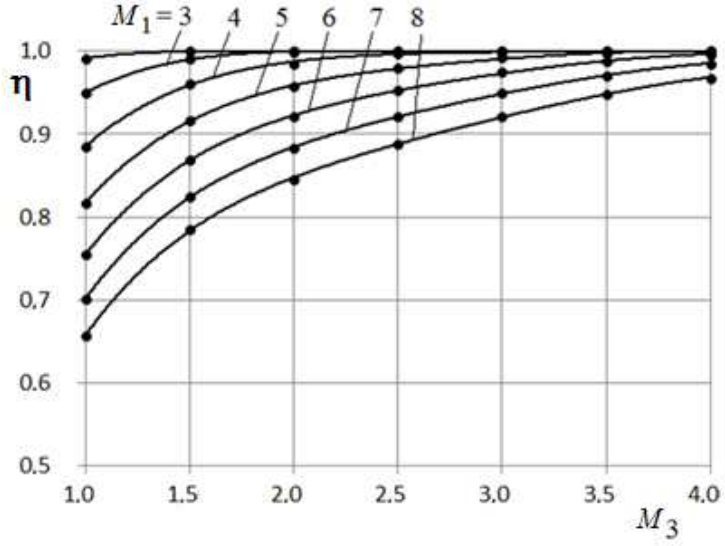

Fig. 6. Total pressure recovery η at the conical shock of the Busemann intake. M_3 is Mach number at the intake exit

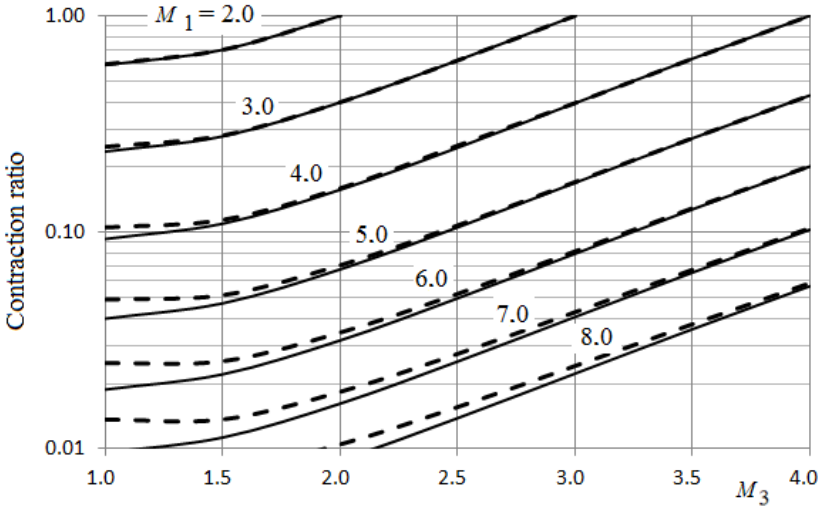

Fig. 7. Contraction ratio in Busemann intake (dashed lines) and in the RIN intake (solid lines). M_3 is Mach number at the intake exit

The contraction ratio of the RIN intake (the reciprocal of the geometric degree of compression of the captured flow) is shown in Fig. 7. The same values of contracting ratio will be implemented for the Busemann intakes. It is seen that at a high speed of the incoming flow, the minimal area of intake exit can be several percent of the captured flow area. The only limitation for obtaining a small intake exit area is the startability problem.

5.2 Calculation inviscid flow

A comparison of the Busemann intake and the RIN intake is shown in Fig. 8. The geometry of the intakes was calculated for the Mach number of the incoming flow M_1 = 6.0 and for the Mach number at the intake exit M_3 = 3.5. Under these conditions, the Busemann intake is shorter than the reversed nozzle intake by 11%.The results for inviscid flow are shown in Table 1 and Table 2.

Table 1. Parameters in the Busemann intake at $M_1 = 6$; $M_3 = 3.5$ is inviscid flow

Busemann	M_1	P_{01}, bar	G_1, kg/s	η	M_3	P_{03}, bar	G_3, kg/s	P_3, bar
Taylor-Maccoll	6.000	1612	78.51	0.9879	3.50	1592	78.51	20.87
CFD	6.000	1609	78.71	0.9847	3.50	1584	78.71	20.68

Table 2. Parameters in the RIN intake at $M_1 = 6$; $M_3 = 3.5$ is inviscid flow

RIN	M_1	P_{01}, bar	G_1, kg/s	η	M_3	P_{03}, bar	G_3, kg/s	P_3, bar
Char	6.000	1612	78.51	1.000	3.50	1612	78.51	21.13
CFD	5.999	1608	78.43	0.996	3.50	1602	78.43	20.91

In Tables 1-2 next designations are used: Taylor-Maccoll - parameters obtained when calculate Busemann intake contour; Char is parameters obtained when calculate RIN intake contour by method of characteristics; CFD - parameters obtained by CFD calculation of the flow inside the fixed profiles without viscosity; P_{01} and P_{03} are stagnation pressures at the entry and exit area; η is total pressure recovery; G_1 and G_3 are the mass flows at the entry and exit area. CFD parameters P_{01}, P_{03}, P_3, η, M_1, M_3, are mass flow averaged values.

Figure 9 and Fig. 10, Tables 1 and 2 show the results of CFD calculations of the flow in the Busemann air intake and in the RIN intake. The flow is inviscid in both air intakes and the parameters of the calculated flow are in good agreement with the values obtained when forming these air intakes. A conical shock is located at the exit of the Busemann air intake, which leads to a total pressure recovery 0.9879, according to theory, and 0.9847, according to the results of CFD calculation. The total pressure recovery at the RIN intake is 0.996 (instead of 1.0).

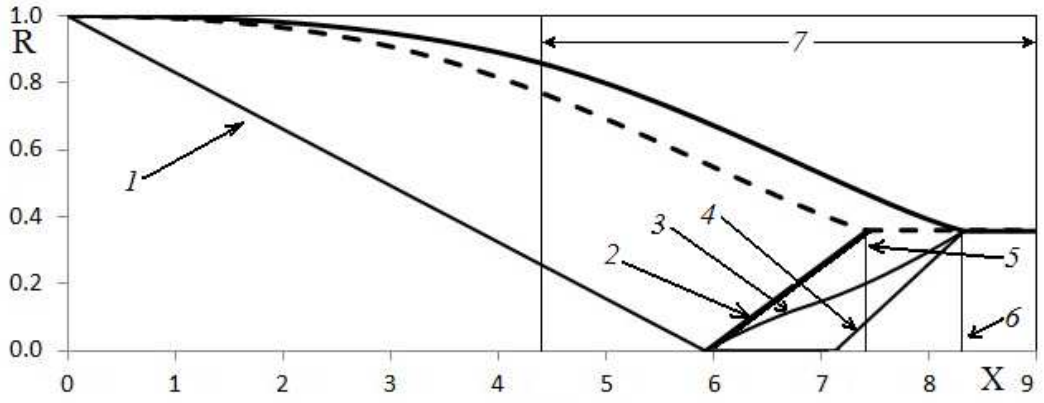

Fig. 8. Comparison of the contours of the Busemann and RIN intakes $M_1 = 6.0$; $M_3 = 3.5$. Solid line is RIN intake (exit area 0.128); dashed line - Busemann intake (exit area 0.129). 1 is uniform characteristic at the entry; 2 is oblique shock in the Busemann intake; 3 is closing characteristic at the corner point in the nozzle; 4 is uniform characteristic in the nozzle; 5 is exit cross section in the Busemann intake; 6 is exit cross section in the RIN intake; 7 is the area of visualization for Fig. 9 – Fig. 12. The linear dimensions (R, X) refer to the entry radius

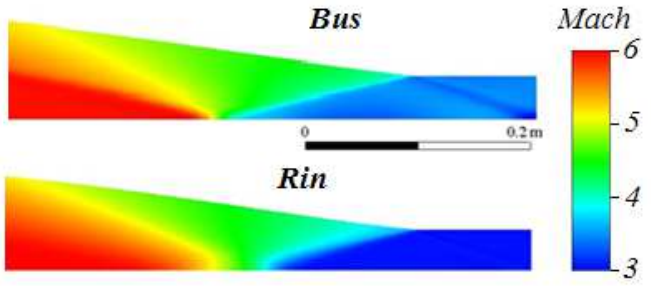

Fig. 9. Results of inviscid flow calculations; $M_1 = 6$; $M_3 = 3.5$. Mach number distribution

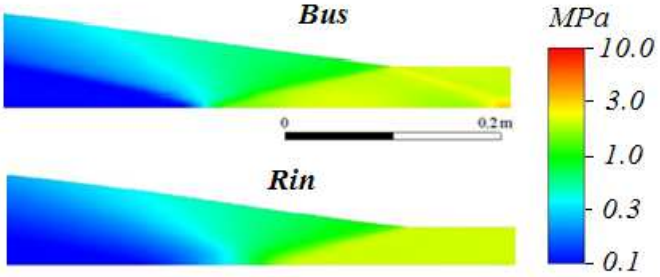

Fig. 10. Results of inviscid flow calculations. $M_1 = 6$; $M_3 = 3.5$. Pressure distribution

Table 3. Parameters in the Busemann intake at $M_1 = 6$; $M_3 = 3.5$

Busemann	M_1	P_{01}, bar	G_1, kg/s	η	M_3	P_{03}, bar	G_3, kg/s	P_3, bar
Taylor-Maccoll	6.000	1612	78.51	0.9879	3.50	1592	78.51	20.87
CFD viscous	5.999	1607	78.71	0.8316	3.18	1404	78.71	26.54

Table 4. Parameters in the RIN intake at $M_1 = 6$; $M_3 = 3.5$

RIN	M_1	P_{01}, bar	G_1, kg/s	η	M_3	P_{03}, bar	G_3, kg/s	P_3, bar
Char	6.000	1612	78.51	1.000	3.50	1612	78.51	21.13
CFD viscous	5.998	1607	78.71	0.869	3.15	1396	78.71	27.27

5.3 Calculation of the viscous flow

Similar CFD calculations were carried out taking into account a turbulent boundary layer on the compression surfaces. The geometry of both intakes was calculated with the Mach number of the incoming flow $M_1 = 6.0$ and the Mach number at the intake exit $M_3 = 3.5$ (see Fig. 8). In Fig. 11 and Fig. 12, as well as in tables 3 and 4, the results of CFD calculations of the flow in the Busemann air intake and in the RIN intake taking into account the viscosity are shown below.
In Tables 3-4 designations are equivalent to Tables 1-2.

There are distinct shock wave/boundary layer interactions in the viscous Busemann intake flow. The conical shock cannot hit the shoulder anymore. The total pressure recovery in compression section is 0.8316 in the Busemann intake and 0.869 in the RIN intake.

6. Conclusion

A new method was proposed for contouring a high speed axisymmetric RIN intake based on the inversion of the flow in a contour supersonic isentropic nozzle with a uniform exit characteristic. A comparison was made on the geometric and gas-dynamic characteristics of the proposed RIN intake and a Busemann intake. A comparison of the characteristics of the two air intakes showed that:

1. The Busemann intake is 23 - 13% shorter than the RIN intake in the range of freestream Mach numbers from $M_1 = 2$ to $M_1 = 8$ due to the presence of the Busemann shock.
2. The losses of the total pressure in the conical shock at the exit of the Busemann intake reach 35% at $M_1 = 8$ and $M_3 = 1$. These losses decrease with increasing M_3 at the exit and become negligible (less than 8%) at $M_3 \geq 3.0$. There is no loss of total pressure in the RIN intake.
3. The flow parameters of CFD calculations without viscosity and boundary layer are in good agreement with the flow parameters obtained when configurations of both types of air intakes were calculated with $M_1 = 6.0$ and $M_3 = 3.5$. The total pressure recovery at the intake exit was 0.9847 (instead of 0.9879 by Taylor-Maccoll equation solution) for the Busemann intake and 0.996 (instead of 1.0 by method of characteristics) for the RIN intake.
4. CFD calculations taking into account viscosity, performed for two air intakes at $M_1 = 6.0$ and $M_3 = 3.5$, showed that the flow parameters at the intake exit are almost the same for the Busemann intake and for the RIN intake due to leveling action of the boundary layer. In this case, the total pressure recovery at the exit is 0.8316 in the Busemann intake and 0.869 in the RIN intake. Due to viscosity the flow parameters are differing from the design values.

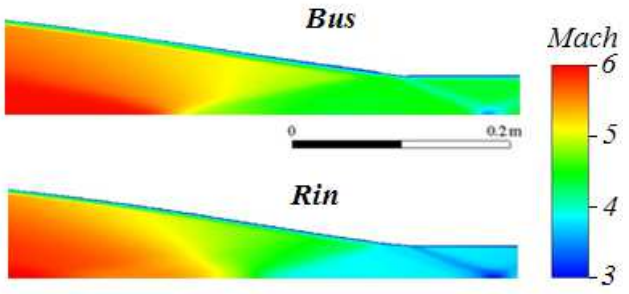

Fig. 11. Results of viscous flow calculations. $M_1 = 6$; $M_3 = 3.5$. Mach number distribution

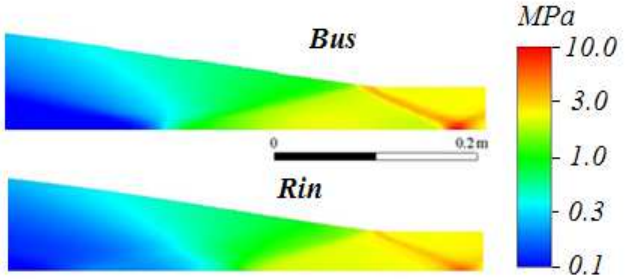

Fig. 12. Results of viscous flow calculations. $M_1 = 6$; $M_3 = 3.5$. Pressure distribution

Authors Contributions

Vladislav Galkin developed the theoretical model of the study, developed the mathematical model; Vasily Fomin initiated the project, conducted the research strategy; Sannu Mölder developed the mathematical modeling and examined the theory validation; Dmitry Vnuchkov performed the mathematical calculations; Valery Zvegintsev supervised the whole research, planned all steps of the project. The manuscript was written through the contribution of all authors. All authors discussed the results, reviewed, and approved the final version of the manuscript.

Acknowledgments

This work was supported in part by the Program of Fundamental Scientific Research for the Academy of Sciences of the Russian Federation in 2013-2020 (project No. AAAA-A17-117030610121-9).

Conflict of Interest

The authors declared no potential conflicts of interest with respect to the research, authorship, and publication of this article.

Nomenclature

H	Total enthalpy
x	Longitudinal axis of the cylindrical coordinate system
y	Transverse axis of the cylindrical coordinate system
ρ	Gas density
u	Components of the gas velocity in the projection on the axis x
v	Components of the gas velocity in the projection on the axis y
p	Gas pressure
γ	Specific heat ratio
δ	Angle between the velocity vector and the x-axis
w	Gas velocity
a	Sound velocity
M	Mach number
μ	Mach angle
$y(x)$	Wall generatrix
$C^{\pm}$	$\pm$Characteristics
M_1	Mach number of uniform flow in maximum section
M_2	Mach number at the front of the shock wave
M_3	Mach number of uniform flow in minimum section
r	Radius vector of spherical coordinates
θ	Spherical angle in spherical coordinates
θ_b	Initial spherical angle
θ_d	Final spherical angle
V_θ	Normal gas velocity to the radius vector
V_r	Tangent gas velocity to radius vector
U	Dimensionless normal gas velocity to the radius vector
V	Dimensionless tangent gas velocity to the radius vector
W_{max}	Maximum gas velocity
P_{01}	Mass flow averaged stagnation pressures at the entry area
P_{03}	Mass flow averaged stagnation pressures at the exit area
G_1	Mass flow rate at the entry area
G_3	Mass flow rate at the exit area
η	Total pressure recovery
L	Length of the intake
D	Diameter of the intake entrance
P	Pressure of incoming flow
T	Temperature of incoming flow
Re_D	Reynolds number based on entry diameter

References

[1] Van Wie, D.M., *Scramjet Intakes: Scramjet Propulsion*, AIAA, 2001.
[2] Van Wie, D.M., Molder, S., Application of Busemann Intake Designs for Flight at Hypersonic Speeds, *Aerospace Design Conference*, Irvine, CA, AIAA Paper, 92-1210, 1992.
[3] Ogawa, H., Mölder, S., Boyce, R., Effects of Leading-Edge Truncation and Stunting on Drag and Efficiency of Busemann Intakes for Axisymmetric Scramjet Engines, *Journal of Fluid Science and Technology*, 8(2), 2013, 186-199.
[4] Timofeev, E.V., Tahir, R.B., Molder, S., On Recent Developments Related to Flow Starting in Hypersonic Air Intakes, *15th AIAA International Space Planes and Hypersonic Systems and Technologies Conference*, Dayton, OH, AIAA, 2008-2512, 2008.
[5] Molder, S., *The Busemann Air Intake for Hypersonic Speeds: Hypersonic vehicles - past, present and future developments*, IntechOpen, 2018.
[6] Busemann, A., Die Achsensymmetrische Kegelige Überschallströmung, *Luftfahrtforschung*, 19, 1942, 137-144.
[7] Flock, A.K., Guelhan, A., Viscous Effects and Truncation Effects in Axisymmetric Busemann Scramjet Intakes, *AIAA Journal*, 54(6), 2016, 1881-1891.
[8] Kraiko, A.N., Tillyaeva, N.I., Axisymmetric-conical and Locally Conical Flows Without Swirling, *Journal of Applied Mechanics and Technical Physics*, 55(2), 2014, 282–298.
[9] Blokhin, A.M., Vetlutskaya, L.M., Gutov, B.I., Dolgov, V.N., Zatoloka, V.V., Shumsky, V.V., Convergent Input Diffusers and Axisymmetric Supersonic Conical Buzemann Flows, *Aerophysical Research, ITAM SB RAS*, 1972, 105–108. (In Russian)
[10] Gutov, B.I., Zatoloka, V.V., Convergent Input Diffusers with an Initial Shock Wave and Additional External Compression, *Aerophysical Research, ITAM SB RAS*, 1973, 64–66. (In Russian)
[11] Gutov, B.I., Zatoloka, V.V., Hypersonic Axisymmetric Compression Flows in Channels Without a Central Body, *Issues of Gas Dynamics, ITAM SB RAS* , 1975, 213–216. (In Russian)
[12] Gounko, Yu.P., Mazhul, I.I., Numerical Modeling of the Conditions for Realization of Flow Regimes in Supersonic Axisymmetric Conical Inlets of Internal Compression, *Thermophysics and Aeromechanics*, 22(5), 2015, 545–558.
[13] Gounko, Yu.P., Mazhul, I.I., Design of Supersonic Three-dimensional Inlets Using Two-dimensional Isentropic Compression Flow, *Thermophysics and Aeromechanics*, 18(1), 2011, 87–100.
[14] Zvegintsev, V., Safonov V., Research of Characteristics of Isentropic Air Intake and Ducted Isentropic Air Intake, *Frontiers in Aerospace Engineering*, 4(2), 2015, 49-55.
[15] Galkin V.M., Zvegintsev, V.I., Forming of Ducted Axisymmetric Supersonic Air Intakes, *Bulletin of the Tomsk Polytechnic University*, 326(4), 2015, 117-124.
[16] Galkin, V.M., Vnuchkov, D.A., Zvegintsev, V.I., Gas-dynamic Design of an Axisymmetric Tunnel Air Inlet with Isentropic Compression, *Journal of Applied Mechanics and Technical Physics*, 56(5), 2015, 111–118.
[17] Galkin, V.M., Zvegintsev, V.I., Vnuchkov, D.A., Investigation of Annular Supersonic Intakes with Isentropic Compression, *Thermophysics and Aeromechanics*, 23(5), 2016, 645-655.
[18] Braguntsov, E.Ya., Vnuchkov, D.A., Galkin, V.M., Ivanov, I.V., Zvegintsev, V.I., Test of the Annular Supersonic Air Intake with Isentropic Compression in the Wind Tunnel, *Tomsk State University Journal of Mathematics and Mechanics*, 43(5), 2016, 43–52.
[19] Taylor, G.I., Maccoll, J.W., The Air-pressure on a Cone Moving at High Speeds, *Proceedings of the Royal Society of London. Series A, Mathematical and Physical Sciences*, 139, 1933, 278-311.
[20] Duncan, W., Tables of Supersonic Flow Around Yawing Cones, *Nature*, 162, 1948, 432-432.
[21] Molder, S., Szpiro, E.J., Busemann Intake for Hypersonic Speeds, *Journal of Spacecraft and Rockets*, 3(8), 1966, 1303-1304.
[22] Molder, S., A Benchmark for Internal Flow CFD Code, *Computational Fluid Dynamics Journal*, 12(2), 2003, 408-414.
[23] Anderson, J.D., *Modern Compressible Flow with Historical Perspective*, McGraw-Hill, Boston, 1990.
[24] Katskova, O.N., *Calculation of Equilibrium Flow within Supersonic Nozzles*, Computing Centre of RAS, Moscow, 1964. (In Russian)
[25] Rao, G.V.R., Exhaust nozzle Contour for Optimum Thrust, *Jet Propulsion*, 28(6), 1958, 377-382.
[26] Ferri A., *Elements of Aerodynamics of Supersonic Flows*, The MacMillan Co., New York, 1949.

[27] Miele A., *Theory of Optimum Aerodynamic Shapes*, Academic Press, New York, 1965.

ORCID iD

Vladislav Galkin https://orcid.org/0000-0002-5359-6253
Vasily Fomin https://orcid.org/0000-0002-2811-0143
Sannu Mölder https://orcid.org/0000-0001-9366-7418
Dmitry Vnuchkov https://orcid.org/0000-0002-8194-5780
Valery Zvegintsev https://orcid.org/0000-0002-4942-9778

How to cite this article: Galkin V., Fomin V., Mölder S., Vnuchkov D., Zvegintsev V. Performance of Two Types of High Speed, High Efficiency Axisymmetric Intakes, *J. Appl. Comput. Mech.*, 7(1), 2021, 93–101. https://doi.org/10.22055/JACM.2020.35250.2609